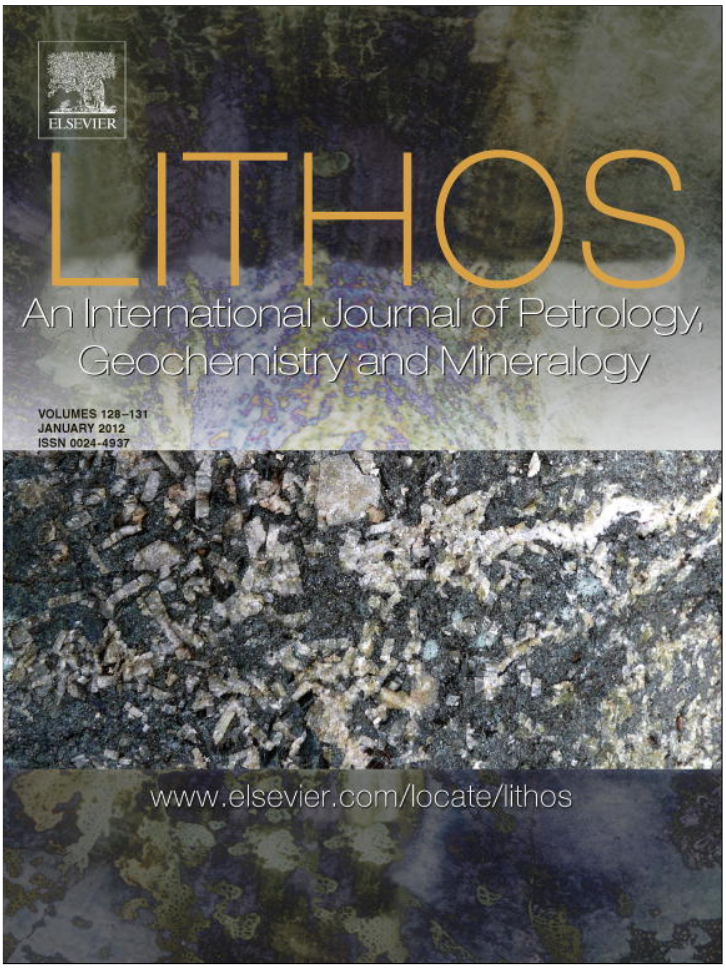

(This is a sample cover image for this issue. The actual cover is not yet available at this time.)

Lithos 144–145 (2012) 12–23

Contents lists available at SciVerse ScienceDirect

Lithos

journal homepage: www.elsevier.com/locate/lithos

Contrasting Triassic ferroan granitoids from northwestern Liaoning, North China: Magmatic monitor of Mesozoic decratonization and a craton–orogen boundary

Xiaohui Zhang [a,*], Lingling Yuan [a,b,c], Fuhong Xue [a,b], Yanbin Zhang [a]

[a] State Key Laboratory of Lithospheric Evolution, Institute of Geology and Geophysics, Chinese Academy of Sciences, Beijing 100029, China
[b] Graduate School of Chinese Academy of Sciences, Beijing 100039, China
[c] China University of Geosciences, Beijing 100083, China

ARTICLE INFO

Article history:
Received 21 January 2012
Accepted 24 March 2012
Available online 31 March 2012

Keywords:
Triassic
Ferroan granite
Crustal growth
Decratonization
North China

ABSTRACT

The diversity exhibited by ferroan granitoids testifies to multiple distinct crustal and mantle processes generally within extensional environments and thus holds the key to monitoring important geodynamic and crustal evolutionary processes and calibrating terrane tectonic affinity. This study documents three Middle to Late Triassic ferroan granitoid suites from northwestern Liaoning, North China, and proposes distinct petrogenetic scenarios for each. The Middle Triassic (ca. 238 Ma) Ping'andi (PAD) granites are mainly calc-alkali and peraluminous. Their radiogenic whole-rock Nd and zircon Hf isotopic signatures argue for an origin consistent with partial melting of a juvenile quartzofeldspathic crust formed by prior mantle-derived magmatic underplating and their differentiations. By contrast, the Late Triassic (ca. 220 Ma) Dashaoleng (DSL) and Sijiazi (SJZ) suites show an evolved character from alkali-calcic to alkali and from metaluminous to peraluminous. Their variably evolved whole-rock Sr–Nd and mixed zircon Hf isotopic compositions suggest that both suites were formed by variable mixing between depleted mantle-derived mafic magma and old crust-derived felsic magma, with distinctively higher input from juvenile components in the DSL suite. These contrasting ferroan granitoid suites not only provide a spatial marker for monitoring juxtaposition of the North China Craton (NCC) and the Central Asian Orogenic Belt (CAOB) along a lithospheric-scale boundary fault in the region, but also present a temporal snapshot that records a southwardly-progressing crustal growth scenario possibly in response to lithospheric dripping within a post-orogenic extensional regime. The cratonic scale synthesis further indicates that diachronous decratonization pattern of the NCC might record episodic response of the craton to evolved plate tectonic processes with two contrasting Phanerozoic orogenic systems.

1. Introduction

Ferroan granitoids, modified from A-type ones (Frost and Frost, 2011) but possibly not limited to the latter, form genetically variable but tectonically consistent intrusive components in most continental tracts of various ages around the world. Their lithological and geochemical diversity testifies to a large variation in potential mantle and crustal sources, conditions of magma formation and evolutionary processes at differing crustal levels (Bonin, 2007; Frost and Frost, 2011; Kemp and Hawkesworth, 2003). They are characteristic of either post-collisional/orogenic extensional regimes or anorogenic within-plate environments (Frost and Frost, 2011 and references therein). Therefore, their genesis holds the key to fingerprinting important geodynamic process (Frost and Frost, 1997; Kemp et al., 2005; Yang et al., 2008a), monitoring continental crustal growth/reworking scenarios (Frost et al., 2001a; Yang et al., 2008b; Zhang et al., 2010a) and calibrating terrane tectonic affinity (Frost et al., 2001a; Zhang et al., 2010a).

As one of the oldest cratons in the world, the North China Craton (NCC) stabilized with the initial formation of a continental root during the Paleoproterozoic (Zhao et al., 2001) and subsequently witnessed the deposition of a thick sequence of Proterozoic to Paleozoic sediments (Kusky et al., 2007; Zhao et al., 2001). Throughout the Phanerozoic era, the NCC was involved in the evolution of circum-cratonic mobile belts. This led to its successive lateral amalgamation with other continental fragments along several collisional orogens and vertical modification of its underlying cratonic roots (Yang et al., 2008b, 2010). Concomitant expressions are multiple episodes of Paleozoic to Mesozoic magmatism along the northern marginal areas of the craton and voluminous Mesozoic magmatism in the eastern part of the craton, with the Triassic being the most significant but poorly documented. Comprehensively characterizing this critical magmatic event and resolving its tectonic affiliation are essential not only for better constraining the on-going controversial Late Paleozoic orogenic cycle along the northern NCC

* Corresponding author. Tel.: +86 10 82998540.
E-mail address: zhangxh@mail.iggcas.ac.cn (X. Zhang).

0024-4937/$ – see front matter © 2012 Elsevier B.V. All rights reserved.
doi:10.1016/j.lithos.2012.03.022

but also for understanding the phenomenal Mesozoic decratonization process in the NCC.

Recent works (Kemp et al., 2005, 2007; Yang et al., 2008a, 2008b) have demonstrated the effectiveness of the integrated whole rock geochemistry and zircon-hosted isotope tracer approach in fingerprinting magma sources and thus in monitoring juvenile crustal addition during magmatic episodes. Herein this approach is employed to unravel contrasting origins for three ferroan granitoid suites from northwestern Liaoning of North China. The results allow us to further evaluate their implications for monitoring decratonization and crustal growth model within the interior of a newly-amalgamated continent consisting of a Precambrian craton and a Phanerozoic orogenic belt.

2. Geological background

With the Central Asian Orogenic Belt (CAOB) to the north and the Qinling–Dabie–Sulu orogenic belt to the south respectively, the NCC comprises two Archean continental blocks (Eastern and Western) separated by the Proterozoic Trans-North China orogenic belt (Zhao et al., 2001) (Fig. 1a). The Eastern and Western blocks developed independently from Late Archean to Early Paleoproterozoic and collided to form a coherent craton at ~1.85 Ga (Zhao et al., 2001). The craton features a basement of dominantly Archean to Paleoproterozoic TTG (tonalitic–trondhjemitic–granodioritic) gneisses and meta-volcanic and sedimentary rocks. Unconformable cover sequences include Mesoproterozoic clastic sedimentary succession of Changcheng System, Cambrian to middle Ordovician marine sedimentary rocks, Carboniferous–Permian continental clastic rocks and Mesozoic basin deposits (Kusky et al., 2007; Zhao et al., 2001).

The east–west trending CAOB consists of island arcs, ophiolites, oceanic islands, accretionary wedges, oceanic plateaux and micro-continents (Windley et al., 2007; Xiao et al., 2003). The northern China–Mongolia tract covers a vast area from southern Mongolia to northern China along the middle-eastern segment of this belt, with the Solonker suture zone being its most prominent tectonic feature (Jian et al., 2010; Xiao et al., 2003; Zhang et al., 2008a). This zone separates two opposite-facing continental blocks and is generally regarded to mark the final closure of the Paleo-Asian Ocean (Fig. 1a) (Jian et al., 2010). Amalgamation of these blocks resulted in a unified North China–Mongolian Plate (Davis et al., 2001).

The northern NCC was a convergent plate margin during the Paleozoic, with several episodes of Ordovician to Permian magmatism developed along the region (Zhang and Zhai, 2010; and references therein). From Early Mesozoic on, it experienced multiple intra-continental tectono-magmatic events, mainly in response to continuing continental contraction along the northern and southern margins of the craton and subduction along its eastern margin (Davis et al., 2001). At least two episodes of contractile tectonism are manifested by regional Jurassic unconformities (at ca. 180 and 160 Ma) and cross-cutting relationships (Davis et al., 2001). Each of these contractional deformation events was followed by several episodes of volcanism, granitoid emplacement and terrestrial deposition. In the Early Cretaceous, the orogenic fabric of the belt was overprinted by widespread extensional features, including a series of metamorphic core complexes (Davis et al., 2001) and rift basins (Cope and Graham, 2007).

Northwestern Liaoning is situated along the eastern segment of the northern NCC (Fig. 1b). It features a Precambrian basement and

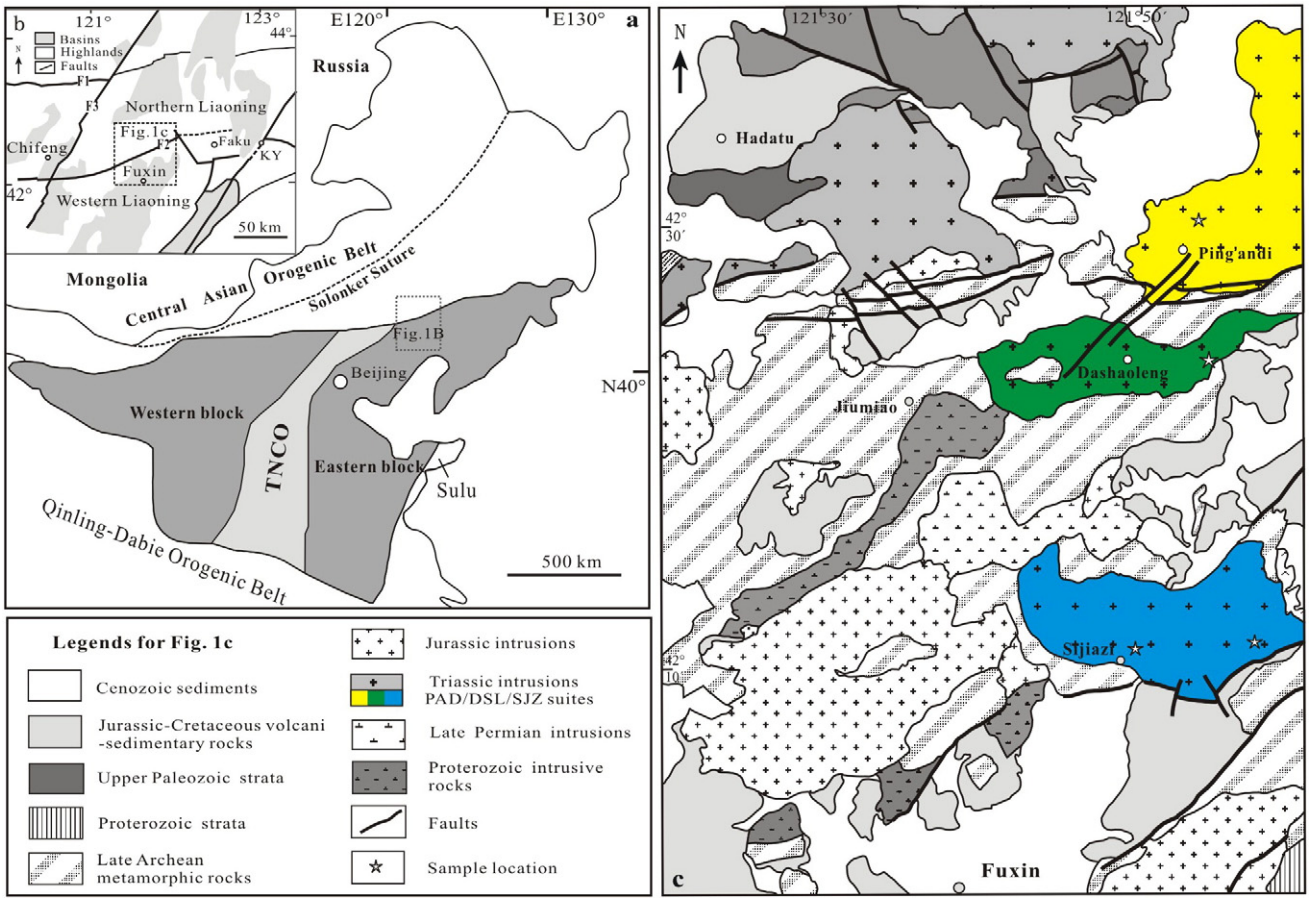

Fig. 1. (a) Simplified map showing major tectonic units of the North China Craton (Zhao et al., 2001). TNCO stands for Trans-North China orogenic belt. (b) Sketch distribution map of the basins and faults in western and northern Liaoning; F1 = Xilamulunhe Fault; F2 = Chifeng–Kaiyuan Fault; F3 = Hongshan–Balihan Fault. (c) Geological sketch map of northwestern Liaoning (modified from LBGMR, 1971), with the sampling locations shown.

Phanerozoic tectonic–magmatic events typical of the NCC (Fig. 1c). The basement comprises lower amphibolite to granulite facies Archean to Paleoproterozoic gray tonalitic gneisses and greenstones of the Jianping complex and Neoproterozoic low-grade metamorphic to unmetamorphosed rock sequences of the Changcheng system. The Jianping complex records a major magmatic event from 2589 to 2495 Ma and a granulite facies metamorphism at ca. 2490 Ma (Liu et al., 2011; Wang et al., 2011). Late Paleozoic marine to continental volcano-sedimentary sequences are sporadically distributed in the northern part of the area. Mesozoic volcanic and continental sedimentary rocks, mainly of Jurassic and Early Cretaceous age, occur primarily in basins developed unconformably on the Archean and Paleoproterozoic basement rocks.

Multiple phases of Phanerozoic igneous rocks intrude Archean and Paleoproterozoic metamorphic rocks at northwestern Liaoning. However, they were not well constrained prior to our present geochronological data. Based on intrusive relationships and mineralogical arguments, they appear to have formed in three episodes: (1) a few Hercynian dioritic to granitic plutons (262–256 Ma, our unpublished data); (2) voluminous Middle–Late Triassic plutonism; and (3) a number of Middle to Late Jurassic granitic intrusions. They are variably covered by Jurassic to Cretaceous volcano-sedimentary strata.

3. Petrography

In this study, we identified three Triassic intrusive complexes from north to south: the Ping'andi (PAD) suite, the Dashaoleng (DSL) suite and the Sijiazi (SJZ) suite. The PAD suite is dominantly composed of monzogranites. Typical samples include 30–35% plagioclase ($An_{14-2}Ab_{83-97}Or_{0-2}$), 35–40% quartz, 25–30% K-feldspar ($Qr_{86-97}Ab_{3-14}$), 3–8% biotite, with accessory zircon, apatite and magnetite. The DSL suite mainly contains fine- to medium-grained granodiorite and monzogranite. Typical granodiorite samples comprise 52–60% plagioclase ($An_{24-1}Ab_{72-98}Or_{0-2}$), 15–20% K-feldspar ($Qr_{82-97}Ab_{3-18}$), 15–20% quartz, 3–6% biotite, 2% hornblende, and accessory zircon, titanite, magnetite and apatite. Typical monzogranite samples contain 35–40% K-feldspar ($Qr_{82-97}Ab_{3-18}$), 30–35% plagioclase ($An_{24-1}Ab_{72-98}Or_{0-2}$), 20–25% quartz, 3–5% biotite, and accessory zircon, apatite, magnetite and titanite. The SJZ suite mainly consists of fine to medium-grained granodiorite and syenogranite, with occasional monzonite. One monzodiorite sample contains 45% plagioclase ($An_{21-1}Ab_{79-97}Or_1$) and 35% orthoclase ($Qr_{82-97}Ab_{3-18}$), subordinate amphibole and accessory apatite, zircon, titanite and opaque oxides. Major constituents for granodiorite include 40–50% plagioclase ($An_{11-1}Ab_{88-99}$), 15–25% quartz, 15–25% perthitic orthoclase ($Qr_{87-98}Ab_{1-13}$), with minor biotite (3%) and accessory zircon, apatite, magnetite, titanite and ilmenite. Major constituents of syenogranite are 40–45% microcline ($Qr_{90-98}Ab_{2-10}$), 30–40% quartz, 15–20% plagioclase ($An_{10-2}Ab_{89-96}$), with minor biotite (3–7%) and accessory zircon, apatite, magnetite and titanite.

4. Analytical methods

Zircons were separated from representative rock samples using standard density and magnetic separation techniques and purified by handpicking under a binocular microscope. Cathodo-luminescence (CL) images were obtained for zircons prior to analyses, using a JXA-8100 microprobe at the Institute of Geology and Geophysics, Chinese Academy of Sciences (IGGCAS), Beijing. to reveal their internal structures. Zircon U/Pb dating was conducted using the Chinese Academy of Sciences Cameca IMS-1280 ion microprobe (CASIMS) at the IGGCAS, following analytical procedures described in Li et al. (2009).

Fresh rock samples were ground in an agate mill to ~200 μm mesh powder for geochemical analyses. For major element determination, mixtures of whole-rock powder (0.5 g) and $Li_2B_4O_7 + LiBO_2$ (5 g) were heated and fused into glass disks and analyzed by X-ray fluorescence spectroscopy (XRF) with a Shimadzu XRF 1500 sequential spectrometer at the IGGCAS. The samples were heated in two steps within separate ovens at 105 °C and 1000 °C respectively to measure loss on ignition (LOI). The analytical uncertainties are better than 5% as revealed by long-term measurements of Chinese national standards GSR-1 (granite) and GSR-3 (basalt).

Trace element abundances were obtained on a VG-PQII ICP-MS also at the IGGCAS. Samples were dissolved in distilled $HF + HNO_3$ in 15 ml high-pressure Teflon bombs at 120°C for 6 days, dried and then diluted with 1% HNO_3 to 50 ml for analysis. A blank solution was prepared and the total procedural blank was <50 ng for all trace elements. Indium was used as an internal standard to correct for matrix effects and instrument drift. Precision for all trace elements is estimated to be 5% and accuracy is better than 5% for most elements, monitored by analyses of Chinese National Standard samples GSR-1 and GSR-3.

Whole-rock Sr and Nd isotopic compositions were measured on a Finnigan Mat 262 thermal ionization mass spectrometer at the IGGCAS, following the procedure described in Zhang et al. (2008a). Procedural blanks were <100 pg for Sm and Nd and <500 pg for Rb and Sr. $^{143}Nd/^{144}Nd$ was corrected for mass fractionation by normalization to $^{146}Nd/^{144}Nd = 0.7219$, and $^{87}Sr/^{86}Sr$ ratios were normalized to $^{86}Sr/^{88}Sr = 0.1194$. The measured values for the BCR-2 Nd standard and BCR-2 Sr standard were $^{143}Nd/^{144}Nd = 0.512641 \pm 0.000010$ (2σ, $n = 4$) and $^{87}Sr/^{86}Sr = 0.705018 \pm 0.000011$ (2σ, $n = 4$) during the period of data acquisition.

In situ zircon Hf isotopic analyses were conducted using the Neptune MC–ICP-MS, equipped with a 193-nm laser at the IGGCAS. Spot size of 32 μm was used for analysis, with a laser repetition rate of 10 Hz at 100 mJ. The detailed analytical procedure and correction for interferences follow those described by Wu et al. (2006). The $^{176}Hf/^{177}Hf$ and $^{176}Lu/^{177}Hf$ ratios of the standard zircon (91500) during analysis were 0.282270 ± 0.000023 (2rn, $n = 15$) and 0.00028, similar to the commonly accepted $^{176}Hf/^{177}Hf$ ratio of 0.282284 ± 0.000003 (1r) measured using the solution method (Woodhead et al., 2004).

5. Results

5.1. Zircon U–Pb data

The results of zircon U–Pb analyses are listed in the online Supplemental Table 1. The zircons from representative rock samples from three suites are mostly euhedral to subhedral, stubby to elongate prisms and commonly show internal oscillatory zoning in CL images (Fig. 2). Fifteen spots for sample PA09-3 from the PAD suite yield Th/U ratios of 0.13–1.59 and define a concordia age of 238.2 ± 2.0 Ma with an MSWD of 1.5 (Fig. 3a). For granite sample DSL09-4 from the DSL suite, eleven analyses on 11 zircon grains result in Th/U ratios of 0.19–2.3 and define a concordia age of 219.6 ± 2.0 Ma with an MSWD of 0.01 (Fig. 3b). For the SJZ suite, sixteen analyzed zircons from monzodiorite sample FX09-1 yield Th/U ratios of 0.48–1.30 and a concordia age of 221.7 ± 1.7 Ma with an MSWD of 0.64 (Fig. 3c); thirteen analyzed zircons for granodiorite sample FX09-2 yield Th/U ratios of 0.35–1.65 and a concordia age of 218.4 ± 1.8 Ma with an MSWD of 0.16 (Fig. 3d); while fifteen analyzed zircons for granite sample FX09-11 yield Th/U ratios of 0.12–1.63 and define a weighted mean $^{206}Pb/^{238}U$ age of 221.3 ± 2.8 Ma with an MSWD of 3.8 (Fig. 3e).

5.2. Geochemical data

Tables 1 (and online Supplemental Table 2), 2 and online Supplemental Table 3 present the whole-rock elemental analyses, Sr–Nd isotopic compositions and zircon Hf isotope data for three suites, respectively. The PAD granites have a restricted SiO_2 range from 75.0 to 76.4% (Fig. 4a), with an Fe-index [$(FeO + 0.9Fe_2O_3)/(FeO + 0.9Fe_2O_3 + MgO)$] of 0.82–0.89 (Fig. 4b), high alkali contents ($K_2O + Na_2O = 7.9$–

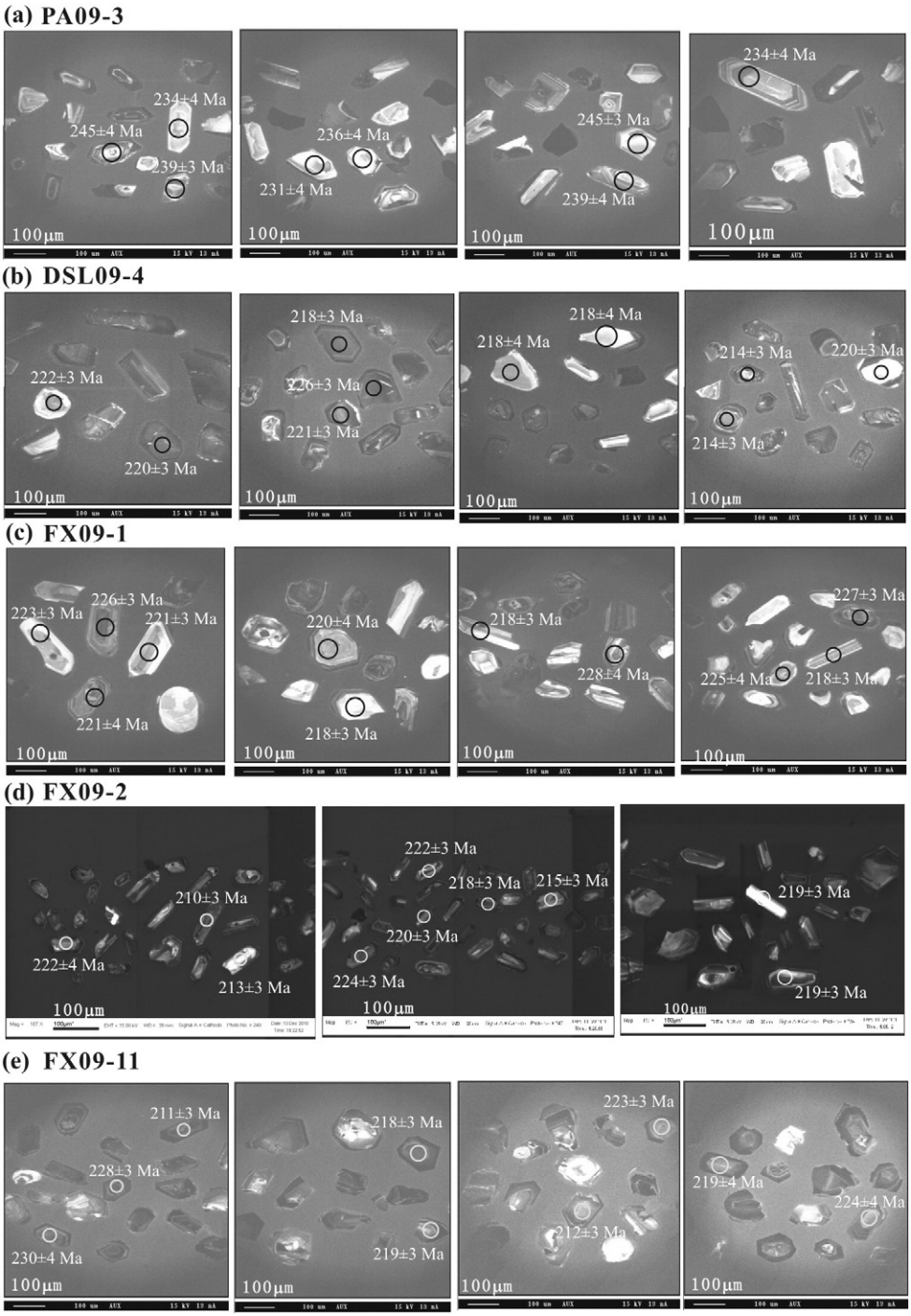

Fig. 2. Cathodoluminescence (CL) images of the dated zircons from three Triassic ferroan granitoid suites from northwestern Liaoning, North China.

8.4%) (Fig. 4c) and a peraluminous character (Fig. 4d). With respect to trace element, they are slightly enriched in light rare earth elements (LREE) with La_N/Yb_N ratios of 1.2–5.5 and minor to moderate Eu anomalies ($Eu/Eu^* = 0.32–0.90$) (Fig. 5a). They show enrichment in both large ion lithophile elements (LILE) and high field strength elements (HFSE) (Fig. 5b). In terms of isotopic composition, the PAD granites exhibit $^{87}Sr/^{86}Sr_i$ ratios from 0.70518 to 0.70538, slightly positive ε_{Nd} (t) values of +0.02 to +0.65 and model ages (T_{DM2}) of 963 to 1007 Ma (Fig. 6a, b). Zircons from sample PA09-3 display a range of initial $^{176}Hf/^{177}Hf$ ratios from 0.28275 to 0.28286, ε_{Hf} (t) values from +4.2 to +8.2 and Hf crustal model ages from 748 to 1002 Ma (Fig. 6c, d).

The DSL suite shows a range in SiO_2 from 67.1 to 73.4% (Fig. 4a), with an Fe-index of 0.82–0.92 (Fig. 4b), high abundances of K_2O (4.54–5.28%) and Na_2O (3.65–6.28%) (Fig. 4c), low contents of CaO (0.26–1.31%) and P_2O_5 (0.04–0.08%), and transitional character from metaluminous to peraluminous (Fig. 4d). The rocks exhibit moderate enrichment in LILE and LREE with La_N/Yb_N ratios of 10.2–16.9 and moderate Eu anomalies ($Eu/Eu^* = 0.31–0.50$), and elevated HFSE (Fig. 5c, d). As for isotopes, they are characterized by $^{87}Sr/^{86}Sr_i$ ratios from 0.70489 to 0.70590, moderately negative ε_{Nd} (t) of −4.80 to −6.35 and model ages (T_{DM2}) of 1386 to 1512 Ma (Fig. 6a, b). Zircons from sample DSL09-4 show an initial $^{176}Hf/^{177}Hf$ ratios from 0.28242 to 0.28293, ε_{Hf} (t) values from −7.8 to +10.2 and crustal Hf model ages between 601 and 1350 Ma (Fig. 6c, d).

The SJZ suite spans a wide range of SiO_2 from 52.1 to 77.4% (Fig. 4a), with Fe-index of 0.79–0.92 (Fig. 4b) and a high-K calc-

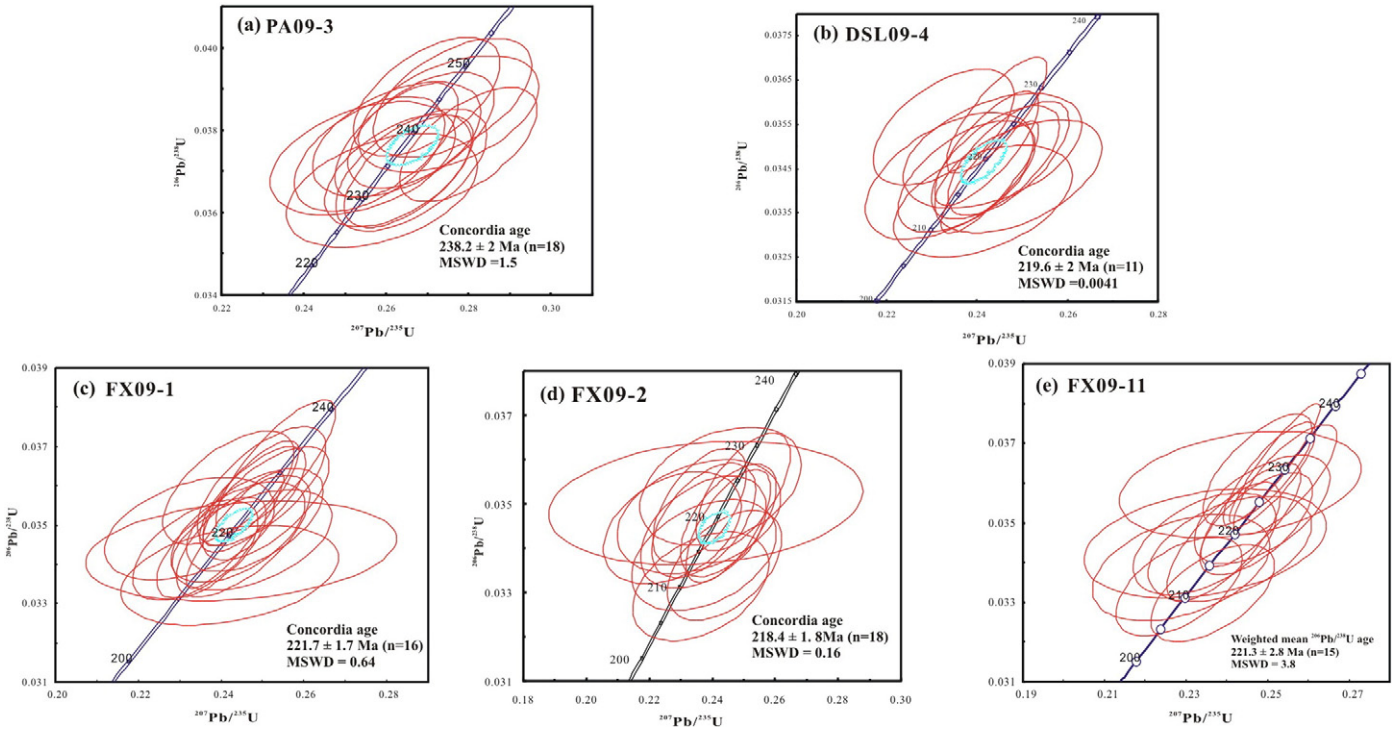

Fig. 3. U–Pb zircon concordia diagrams for three Triassic ferroan granitoid suites from northwestern Liaoning, North China.

alkaline affinity for dominant felsic samples. One monzodiorite sample exhibits high MgO (5.98%) and Fe_2O_3 (6.11%), as well as elevated Mg# (67), Cr (353 ppm) and Ni (153 ppm). It features a $^{87}Sr/^{86}Sr_i$ ratio of 0.70495, slightly positive ε_{Nd} (t) of +0.62 and model age of 953 Ma (Fig. 6a, b). Zircons from sample FX09-1 exhibit a wide range of initial $^{176}Hf/^{177}Hf$ ratios from 0.28174 to 0.28283, ε_{Hf} (t) values from −31.8 to +6.9 and crustal model ages from 819 to 3269 Ma (Fig. 6c, d). The other rocks from the suite define a continuous chemical evolutionary trend, from less-differentiated low-silica granodiorite displaying LREE enriched patterns, moderate negative Eu anomalies and high Zr and Hf, to more-differentiated, high-silica granites with higher alkalis, low abundance of LREE and Zr, strong depletion in Ba, Sr and Ti (Fig. 5e, f). In terms of isotopic composition, they display $^{87}Sr/^{86}Sr_i$ ratios from 0.70225 to 0.70770, negative ε_{Nd} (t) of −8.94 to −9.12 and model ages of 1729 to 1798 Ma (Fig. 6a, b). Zircons from granodiorite sample FX09-2 exhibit a range of initial $^{176}Hf/^{177}Hf$ ratios from 0.28205 to 0.28271, ε_{Hf} (t) values from −20.9 to +2.8, and Hf crustal model ages from 1078 to 2563 Ma, while those from granite sample FX09-11 exhibit a range of initial $^{176}Hf/^{177}Hf$ ratios from 0.28244 to 0.28255, ε_{Hf} (t) values from −3.0 to −6.9 and Hf crustal model ages from 1448 to 1692 Ma (Fig. 6c, d).

6. Discussion

6.1. Contrasting magmatic affinity

As the most popular one among approximately 20 different granite classification schemes evolved over the past several decades, the Alphabetic classification subdivides granitoids into I-, S-, M- and A-types in terms of their protolith nature (Pitcher, 1993). However, distinction between these types is not always straightforward, given the fact that similar granitic compositions can be produced by partial melting of a variety of sources or can be achieved by a number of processes (e.g., Frost et al., 2001b). This is true for the present granitic rocks. On the $K_2O + Na_2O$, FeO_t/MgO and Nb vs. Ga/Al diagrams of Whalen et al. (1987), the PAD granites straddle the fields of A-, M-, I-, S-types, whereas most samples from the DSL and SJZ plot within the A-type granite field (Fig. 7a and online Supplemental Fig. 1). On the FeO_t/MgO and $(K_2O + Na_2O)/CaO$ vs. $(Zr + Nb + Ce + Y)$ diagrams of Whalen et al. (1987), similar distribution trends persist, with the PAD granites plotting on the fractionated felsic I-type field but most DSL and SJZ rocks on the A-type granite field (Fig. 7b and online Supplemental Fig. 1). On the R2 versus R1 diagram of Batchelor and Bowden (1985), the PAD granites cluster in the transitional area between syn-collisional and post-orogenic fields, while the DSL and SJZ samples scatter among late-orogenic, post-orogenic and anorogenic fields (Fig. 7c). On the Rb vs. Y + Nb diagram of Pearce et al. (1984), the rocks from these three plutons plot in both the VAG (volcanic arc granite) and WPG (within-plate granite) fields but consistently fall in the post-collisional field of Pearce (1996) (Fig. 7d).

Noting the limitations of previous granite classification schemes, Frost et al. (2001b) proposed a non-genetic, non-tectonic geochemical classification scheme that incorporates some of the best qualities of the previous schemes. Although not unanimously accepted, this scheme provides a mutually exclusive and collectively exhaustive way of geochemically characterizing various granitoids from late-orogenic to intraplate tectonic regimes. According to this three-tiered scheme, the PAD granites are ferroan, calc-alkali and peraluminous (Fig. 4b, c, d), while both the DSL and SJZ suites are ferroan, alkali-calcic to alkali and range from metaluminous to peraluminous (Fig. 4b, c, d).

6.2. Granite genesis

Multiple petrogenetic models have been proposed for the origin of various ferroan granitoids (Frost and Frost, 2011; and references therein), including (1) extreme differentiation of mantle-derived basaltic magma; (2) partial melting of quartzofeldspathic crustal rocks; (3) the integration of crustal and mantle sources, in the form either of crustal assimilation and fractional crystallization (AFC) of mantle-derived basaltic magmas, or of mixing between mantle-derived and crustal magmas.

For the PAD granites, the relative scarcity of intermediate and mafic members in the suite and their peraluminous character is

Table 1
Major and trace element data for representative samples from three Triassic ferroan granitoid suites from northwestern Liaoning, North China.

Sample	PA09-01	PA09-02	DSL09-01	DSL09-05	FX09-01	FX09-02	FX06-8	FX09-11
Longitude and latitude	E121°52′59 N 42°30′31		E121°53′13″ N 42°23′31		E121°50′49 N 42°11′25		E121°57′16 N 42°11′10	
SiO_2	75.17	75.78	68.39	73.40	52.07	62.86	71.79	76.68
TiO_2	0.08	0.06	0.24	0.27	0.72	0.33	0.27	0.08
Al_2O_3	13.91	13.81	16.05	14.09	16.92	18.34	13.92	12.88
TFe_2O_3	0.83	0.60	2.48	1.40	6.11	2.12	1.73	0.61
MnO	0.02	0.03	0.05	0.03	0.09	0.01	0.03	0.01
MgO	0.13	0.10	0.23	0.28	5.98	0.16	0.42	0.05
CaO	0.90	0.81	1.01	0.50	4.68	0.85	1.28	0.42
Na_2O	4.08	3.94	5.81	3.91	5.43	5.61	3.64	3.89
K_2O	4.28	4.38	4.69	5.09	1.24	7.35	5.01	4.57
P_2O5	0.02	0.01	0.06	0.07	0.19	0.06	0.06	0.01
LOI	0.66	0.60	0.36	1.02	6.76	1.74	1.18	0.44
Total	100.08	100.12	99.37	100.05	100.19	99.42	99.33	99.64
Mg#	23.7	24.8	15.5	28.4	66.0	13.0	32.4	14.0
A/CNK	1.07	1.09	0.97	1.10	0.90	0.98	1.01	1.06
Sc	3.19	2.59	3.30	4.98	16.8	4.89	2.05	3.15
V	8.10	7.14	12.6	19.5	108	11.2	14.6	8.59
Cr	2.75	1.52	5.27	2.78	353	3.17	3.13	2.90
Co	1.13	0.99	2.28	2.26	28.9	2.59	2.07	0.95
Ni	4.84	0.48	16.9	1.66	157	2.16	2.31	5.96
Ga	18.3	16.6	20.6	23.9	20.8	17.18	17.4	17.0
Rb	205	184	211	239	38.5	274	218	185
Sr	200	162	150	159	448	214	198	41.4
Y	22.8	21.3	26.9	25.0	12.1	41.1	25.2	2.91
Zr	77.7	68.7	230	274	130	292	201	79.6
Nb	22.8	21.0	46.0	29.7	5.32	31.8	23.8	11.5
Cs	4.03	3.29	3.34	3.78	0.77	3.61	4.93	4.17
Ba	514	457	536	685	387	1083	714	99.7
Hf	2.87	2.44	8.47	7.27	3.71	8.63	5.65	2.96
Ta	1.82	2.44	4.31	3.42	0.41	3.63	2.73	0.96
Pb	26.8	24.8	22.9	28.1	18.6	23.6	27.1	26.6
Th	15.8	8.08	47.3	30.9	7.39	55.3	41.0	15.3
U	2.24	1.88	8.47	14.0	1.70	8.38	6.53	1.12
La	17.4	7.79	64.8	54.5	21.6	81.8	57.8	15.5
Ce	30.2	11.2	114	97.3	41.8	150	100	38.7
Pr	3.87	1.76	12.0	10.4	5.29	15.2	10.5	2.32
Nd	14.3	6.85	39.4	34.6	19.9	50.2	35.7	5.88
Sm	3.39	1.70	6.01	5.34	4.13	8.33	5.60	0.76
Eu	0.43	0.33	0.68	0.81	1.10	1.08	0.74	0.16
Gd	3.39	1.89	5.49	4.99	3.31	8.12	4.79	0.68
Tb	0.66	0.42	0.79	0.73	0.47	1.28	0.72	0.09
Dy	4.19	3.26	4.39	4.05	2.53	7.40	4.16	0.56
Ho	0.85	0.77	0.94	0.88	0.48	1.51	0.84	0.12
Er	2.30	2.56	2.75	2.61	1.30	4.02	2.36	0.39
Tm	0.35	0.45	0.45	0.40	0.20	0.59	0.37	0.07
Yb	2.24	3.12	3.06	2.75	1.31	3.72	2.50	0.52
Lu	0.34	0.52	0.48	0.41	0.20	0.54	0.37	0.09
La_N/Yb_N	5.58	1.79	15.2	14.2	11.8	15.8	16.6	21.2
Eu/Eu^*	0.38	0.56	0.36	0.48	0.91	0.40	0.44	0.68

Notes: Mg# = 100 × molar Mg/(Mg + Fe) ($TFeO = 0.9 \times TFe_2O_3$); LOI = loss on ignition; A/NCK = Al/Na + Ca + K; $Eu/Eu^* = Eu_N/[(Sm_N + Gd_N)/2]$; N = chondrite normalized to values of Sun and McDonough (1989).

obviously at odds with a magma differentiation model that commonly features a closely-related low-silica suite and results in metaluminous products (Frost and Frost, 2011; Whitaker et al., 2008). Meanwhile, their uniform positive whole-rock ε_{Nd} (t) and zircon ε_{Hf} (t) values negate any hybridization process that would produce felsic melts with variable isotopic signatures. These preclusions narrow our choice down to a crustal anatexis scenario. As demonstrated by both numerous experimental works (Bogaerts et al., 2006; Patiño Douce, 1997; Skjerlie and Johnston, 1993) and type examples (Frost and Frost, 2011 and references therein), dehydration melting of quartzofeldspathic crust under relatively oxidizing conditions could yield geologically important volumes of ferroan, calc-alkaline granitic magmas with negative Eu anomalies and homogeneous isotopic imprints. Furthermore, the radiogenic whole-rock Nd and zircon Hf isotopic compositions in the PAD suite are more compatible with a juvenile crustal protolith than cratonic source of substantial crustal residence age. This is closely analogous to the coeval Faku calc-alkaline to alkaline granites from the neighboring northern Liaoning (Zhang et al., 2010a), whose parental magmas are interpreted to contain significant juvenile materials with a provenance affinity of CAOB. Therefore, we suggest that the parental magma for the PAD suite most likely originated from partial melting of a CAOB-style mixed protolith composed of dominant juvenile underplates and minor old crustal materials (Fig. 6b).

By contrast, the DSL and SJZ suites show a broad range of zircon ε_{Hf} (t) values from moderately positive to highly negative (Fig. 6c, d) and variable Hf crustal model ages. Such variable isotopic signatures commonly argue for a hybridization petrogenetic scenario (Griffin et al., 2002; Kemp et al., 2007; Yang et al., 2008a,b). Of potential source contributors in our case, mantle-derived mafic magma end-member is represented by unusual monzodiorite sample FX09-1 from the SJZ suite. With its radiogenic whole-rock Nd and zircon Hf isotopic composition, it seems to contradict with the moderately enriched character of the subcontinental lithospheric mantle beneath the northern NCC during Early Mesozoic times. As constrained by the Late

Table 2
Rb–Sr and Sm–Nd isotopic compositions for three ferroan granitoid suites from northwestern Liaoning, North China.

Sample no.	Rb [ppm]	Sr [ppm]	$^{87}Rb/^{86}Sr$	$^{87}Sr/^{86}Sr$	(2σ)	$^{87}Sr/^{86}Sr_i$	Sm [ppm]	Nd [ppm]	$^{147}Sm/^{144}Nd$	$^{143}Nd/^{144}Nd$	(2σ)	Initial Nd	ε_{Nd} (t)	T_{DM} (Ma)	T_{DM2} (Ma)
Ping'andi suite (t = 238 Ma)															
PA09-2	180.0	152.5	3.420	0.716758	13	0.705180	1.49	5.90	0.1528	0.512598	11	0.512360	+0.55	1380	963
PA09-3	170.4	148.7	3.321	0.716419	12	0.705176	1.39	5.14	0.1634	0.512605	12	0.512350	+0.37	1648	977
PA09-6	190.4	143.2	3.854	0.718241	11	0.705194	1.85	7.89	0.1420	0.512586	14	0.512348	+0.65	1198	956
PA09-8	163.1	196.7	2.401	0.713511	11	0.705383	1.20	5.05	0.1432	0.512556	11	0.512326	+0.02	1283	1007
Dashaoleng suite (t = 220 Ma)															
DSL09-2	213.8	148.5	4.172	0.718956	12	0.705902	5.23	32.4	0.0978	0.512244	11	0.512103	−4.91	1191	1395
DSL09-4	215.5	135.6	4.605	0.720167	11	0.705758	6.08	40.0	0.0920	0.512238	15	0.512106	−4.87	1142	1392
DSL09-5	226.3	154.4	4.246	0.718170	11	0.704885	4.81	29.9	0.0972	0.512195	15	0.512055	−5.85	1248	1472
DSL09-7	232.5	136.7	4.930	0.720892	18	0.705467	5.34	30.8	0.1049	0.512260	12	0.512109	−4.80	1246	1386
DSL09-13	220.2	190.1	3.355	0.715954	11	0.705457	4.68	29.5	0.0961	0.512168	12	0.512030	−6.35	1272	1512
Sijiazi suite (t = 220 Ma)															
FX09-1	35.8	416.7	0.2485	0.705731	11	0.704953	3.58	18.2	0.1191	0.512553	11	0.512374	+0.62	962	953
FX09-11	171.4	36.3	13.74	0.745240	10	0.702249	0.69	5.72	0.0731	0.511985	14	0.511875	−9.12	1262	1746
FX06-9	251.1	151.9	4.7884	0.720977	12	0.705995	6.117	38.60	0.0958	0.511986	12	0.511826	−9.44	1502	1792
FX06-12	189.0	194.8	2.8091	0.716489	13	0.707700	5.970	40.88	0.0883	0.511970	13	0.511823	−9.51	1432	1798
FX06-11	266.4	240.0	3.2154	0.716352	9	0.706291	7.054	37.37	0.1141	0.512056	13	0.511884	−8.94	1670	1729
FX06-14	263.2	181.7	4.1982	0.717854	11	0.704718	5.642	35.57	0.0959	0.512014	13	0.511876	−9.35	1467	1756

Notes: $^{87}Sr/^{86}Sr_i = (^{87}Sr/^{86}Sr)_{sample} - (^{87}Rb/^{86}Sr)_{sample} \times (e^{\lambda t} - 1)$, $\lambda = 1.42 \times 10^{-11}$ year^{-1} (Steiger and Jäger, 1977); initial Nd $= (^{143}Nd/^{144}Nd)_{sample} - (^{147}Sm/^{144}Nd)_{sample} \times (e^{\lambda t} - 1)$, $\varepsilon_{Nd} = ((^{143}Nd/^{144}Nd)_{sample}/(^{143}Nd/^{144}Nd)_{CHUR} - 1) \times 10{,}000$, $f_{Sm/Nd} = (^{147}Sm/^{144}Sm)_{sample}/(^{147}Sm/^{144}Sm)_{CHUR} - 1$, $T_{DM1} = 1/\lambda \times \ln(1 + ((^{143}Nd/^{144}Nd)_{sample} - 0.51315)/((^{147}Sm/^{144}Nd)_{sample} - 0.2137)$, where $(^{147}Sm/^{144}Nd)_{CHUR} = 0.1967$, $(^{143}Nd/^{144}Nd)_{CHUR} = 0.512638$, $\lambda_{SM} = 6.54 \times 10^{-12}$ year^{-1} (Lugmair and Marti, 1978); $T_{DM2} = T_{DM1} - (T_{DM1} - t) \times (f_{cc} - f_{sample})/(f_{cc} - f_{DM})$, where $f_{cc} = -0.4$, $f_{DM} = 0.0859$.

Permian mafic–ultramafic intrusions from the study area (Fig. 6d; our unpublished data) and by multiple episodes of Late Paleozoic mantle-derived mafic magmas from the northern NCC (Zhang et al., 2009a,b, 2011a, 2012a), such EM1-type lithospheric mantle generally features unradiogenic Nd [ε_{Nd} (t) < −6] and zircon Hf [ε_{Hf} (t) < −8] isotopic compositions and is involved in the formation of the Triassic alkaline rocks from the hinterland of the NCC (Ying et al., 2011). Instead, the mafic sample from the SJZ suite bears close resemblance to the coeval gabbroic rocks from the neighboring northern Liaoning with a CAOB tectonic affinity (Zhang et al., 2009c, 2010a). This indicates that a similar juvenile lithospheric mantle could have been involved in the formation of the present rocks. Such a mantle component has also

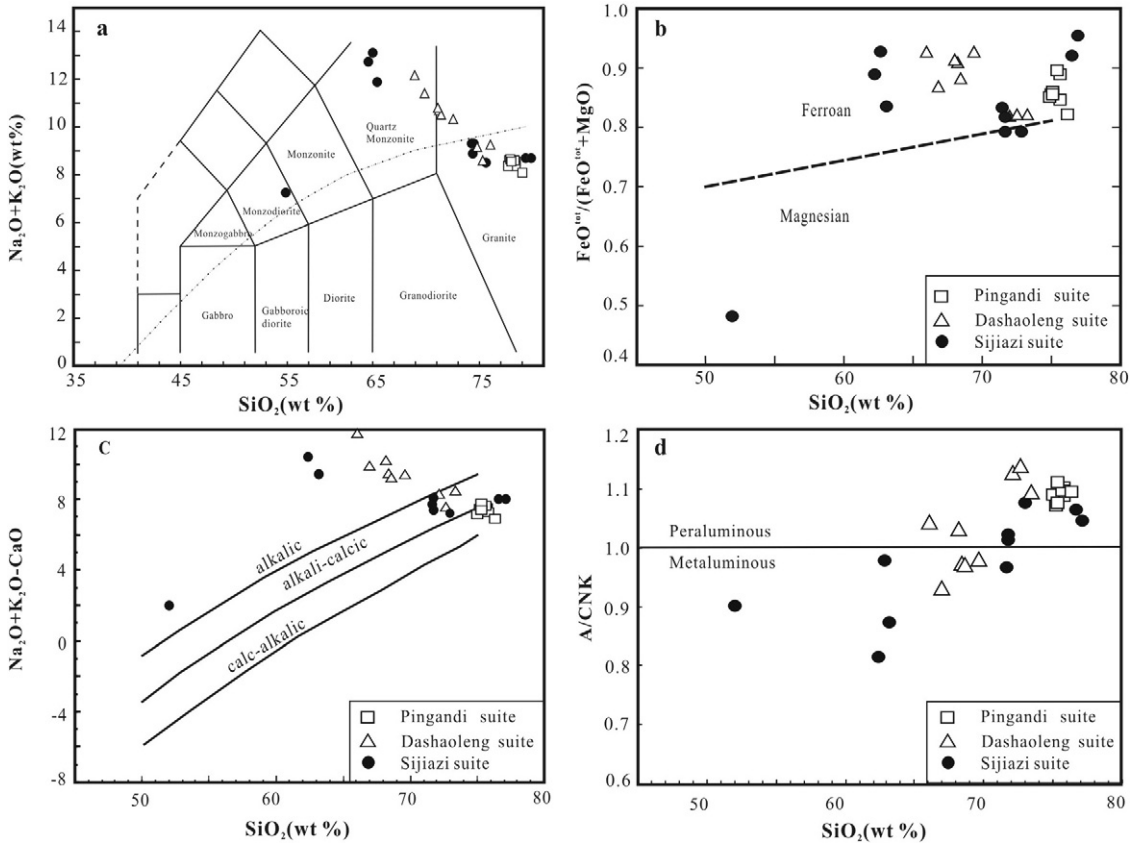

Fig. 4. Classification diagrams for three Triassic ferroan granitoid suites from northwestern Liaoning, North China. (a) Total alkalis vs. silica (Le Maitre, 2002). (b) Plot of $FeO_t/(FeO_t + MgO)$ vs. SiO_2 (Frost et al., 2001b). (c) Plot of $Al_2O_3/(CaO + Na_2O + K_2O)$ calculated on a molecular basis (A/CNK) against SiO_2. (d) Plot of $(Na_2O + K_2O–CaO)$ vs. SiO_2 (Frost et al., 2001b).

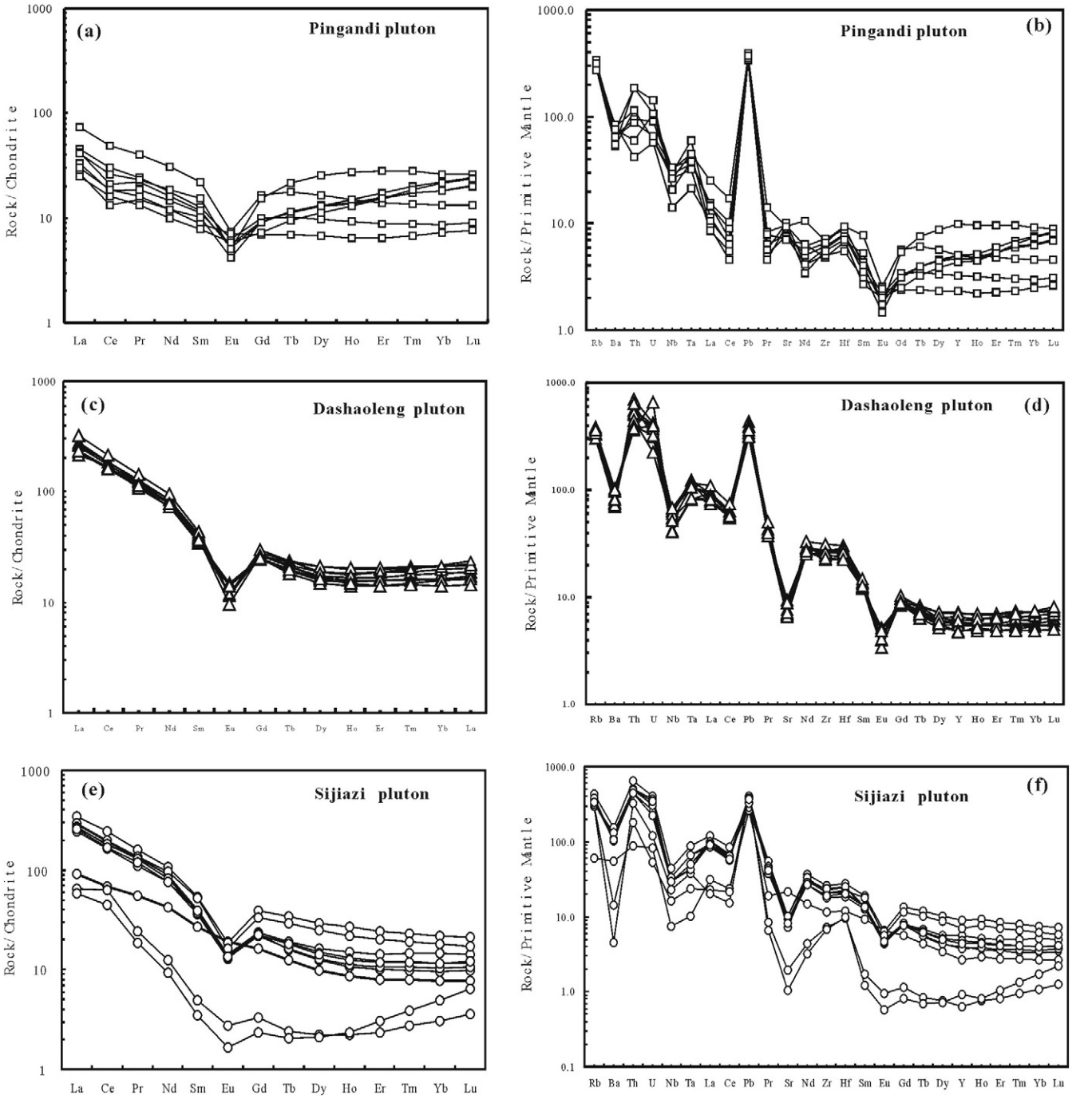

Fig. 5. Chondrite-normalized REE patterns (a), (c), (e) and Primitive mantle-normalized trace element spidergrams (b), (d), (f) for the PAD, DSL and SJZ suites, respectively. Normalization values are from Sun and McDonough (1989).

been documented in the Triassic shoshonitic dykes (Fu et al., 2012) and mafic enclave-bearing A-type granites (Zhang et al., 2012b) from other regions of the northern NCC.

For the felsic magma end-member, extremely low zircon ε_{Hf} (t) values down to −30 in some felsic samples point to an ancient lower crust origin, akin to pure crust-derived felsic magmas as represented by the Jurassic Lüshan granites from western Liaoning (Zhang et al., 2008b) and ancient crustal ingredients involved in the Cretaceous alkaline rocks from the northern NCC (Yang et al., 2008a).

Given the existence of contemporaneous mantle-derived mafic melts, an AFC process could have been responsible for the formation of the DSL and SJZ suites, similar to the alkaline magmatic suite of the Amram Massif (Mushkin et al., 2003). However, its application to the current situation presents serious challenges. First, the felsic rocks in these suites overwhelmingly outnumber the mafic ones. Second, the large variations in zircon ε_{Hf} (t) values with uniform Triassic ages, preclude crustal assimilation, but support magma mixing (Belousova et al., 2006; Griffin et al., 2002; Yang et al., 2008a). Third, recent experimental work demonstrated that extreme fractionation (96–97 vol.%) would be required for a mafic parental magma to yield residual liquids of potassic, low-silica rhyolitic composition ($\leq$68 wt.% SiO_2), with the most voluminous products being intermediate in composition (Sisson et al., 2005; Whitaker et al., 2008). The relative scarcity of intermediate rocks in the DSL and SJZ suites is obviously inconsistent with a simple magma differentiation model, after all, intermediate liquids with lower viscosity than granitic liquids would have intruded to the present level

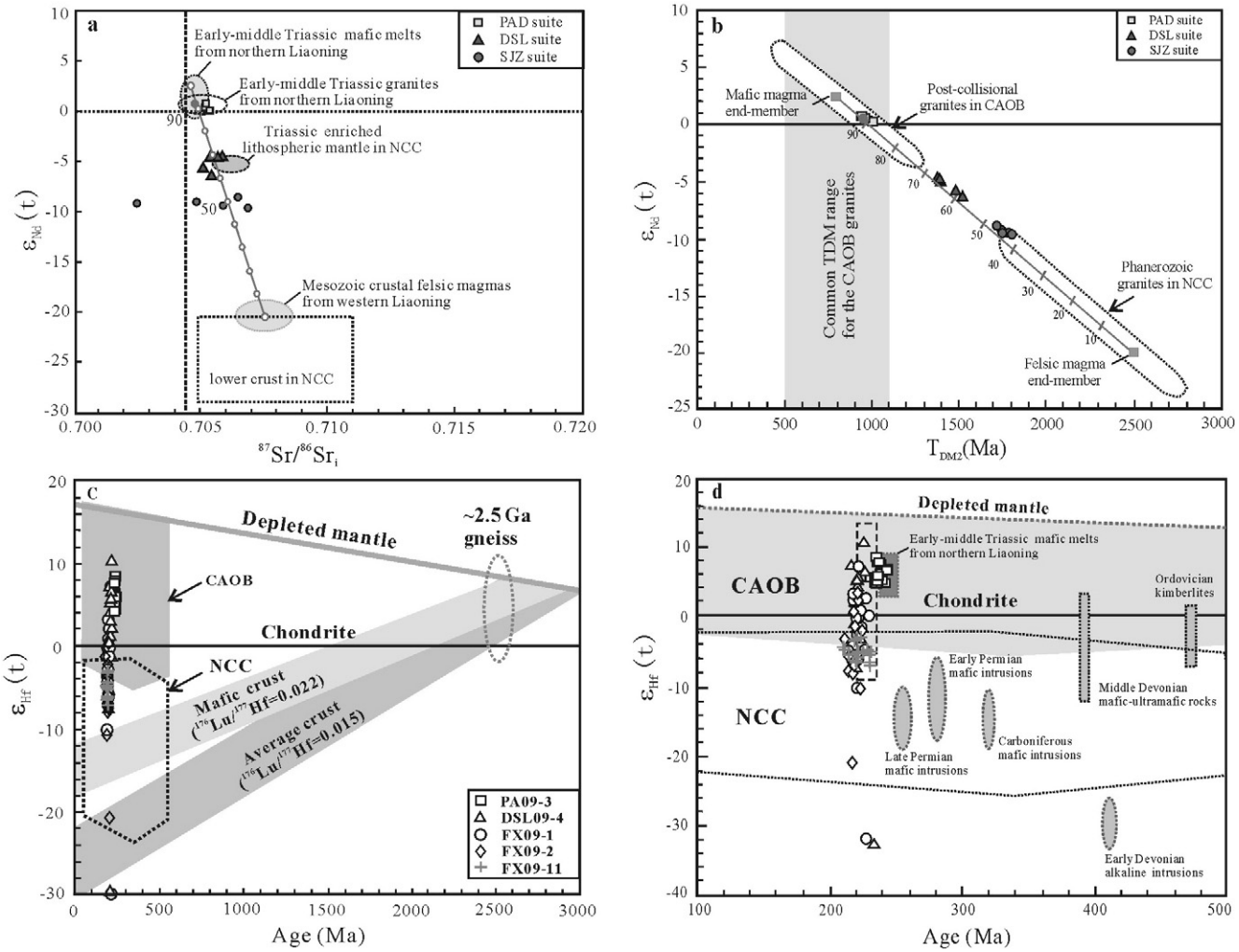

Fig. 6. Plots of (a) ε_{Nd} (t) vs. $^{87}Sr/^{86}Sr_i$, (b) ε_{Nd} (t) vs. T_{DM2}, (c) zircon ε_{Hf} (t) vs. U–Pb age from 0 to 3000 Ma and (d) zircon ε_{Hf} (t) vs. U–Pb age from 100 to 500 Ma for three Triassic ferroan granitoid suites from northwestern Liaoning, North China. In (a), Early–Middle Triassic mafic and felsic melts from northern Liaoning are from Zhang et al. (2009c, 2010a). The Mesozoic crust-derived felsic magma from western Liaoning is from Zhang et al. (2008b). The Triassic enriched lithospheric mantle is from Ying et al. (2011). The parameters used in the mixing modeling are as follows: depleted mantle-derived magma end-member: $^{87}Sr/^{86}Sr = 0.7048$, $\varepsilon_{Nd} = 2.5$; crust-derived felsic magma end-member: $^{87}Sr/^{86}Sr = 0.7075$, $\varepsilon_{Nd} = -20$. In (b), Common T_{DM2} range for the CAOB granites is from Jahn (2004). In (c), Fields for the CAOB and NCC are from Yang et al. (2006). The field for Archean gneiss is from Liu et al. (2011) and Wang et al. (2011). In (d), Fields for Ordovician kimberlites, Early Devonian alkaline intrusions, Middle Devonian mafic–ultramafic rocks, Carboniferous and Early Permian mafic intrusions from the northern NCC are from Yang et al. (2009), Zhang et al. (2010b), Zhang et al. (2009a), Zhang et al. (2012a) and Zhang et al. (2011a), respectively. Field for Late Permian mafic intrusions from the study area is from our unpublished data. Dark gray rectangular area indicates zircons from Early to Middle Triassic mafic intrusions in northern Liaoning (Zhang et al., 2009c, 2010a). Dashed line area represents detrital zircons from the Xinglonggou formation in the northwestern Liaoning (Meng et al., 2010).

(Clemens et al., 2009). Fourth, recent thermal simulations showed that bulk assimilation processes (both mechanical and reactive) could suffer from severe energy barriers, with maximum amount of assimilation at optimum conditions unlikely exceeding ~25% (Glazner, 2007).

With these arguments against bulk assimilation process and numerous case examples of magma mixing involving two or more melt components (Clemens et al., 2009; Kemp et al., 2007; Shaw and Flood, 2009; Yang et al., 2008a; Ying et al., 2011), we prefer a magma mixing scenario between two silicic melts in a deep crustal hot zone for the genesis of the DSL and SJZ suites, as is also evidenced by the occurrence of mafic microgranular enclaves in the DSL suite (LBGMR, 1996).

This can be quantitatively tested by simple mixing models based on the Sr–Nd isotopes of potential end-members. Modeling results show that the DSL rocks are consistent with mixing between 30–40% ancient crust-derived felsic melts and 60–70% depleted mantle-derived magmas, whereas a higher percentage participation of ancient crustal felsic melts (50–60%) in the mixing (Fig. 6a, b), coupled with subsequent fractional crystallization of a hybrid parental magma, can explain the geochemical variations of the SJZ suite.

6.3. Tectonic implications

With their distinct geochemical signatures and contrasting origins, the present three Triassic ferroan granitoids attest to a complex tectonic setting of northwestern Liaoning at the confluence of several lithospheric-scale boundary faults. On one hand, the juvenile character of the PAD suite points to a tectonic affinity with the Phanerozoic accretionary orogenic belt (Fig. 6c); on the other hand, mixed geochemical signatures in the DSL and SJZ suites reflect variable but a consistent cratonic contribution. This disparity implies that the CAOB and NCC juxtaposed along the Chifeng–Kaiyuan Fault (F2 on Fig. 1b) but not the Xilamulunhe Fault (F1 on Fig. 1b), echoing the suggestion from the tectonic reconstruction in northern Liaoning (Zhang et al., 2010a) and thus ensuing the settlement of a long-term controversial regional tectonic issue.

Like their coeval counterparts from northern Liaoning (Zhang et al., 2009c, 2010a), the strong juvenile isotopic imprint in the PAD suite records significant crustal growth. By contrast, the largely positive zircon ε_{Hf} (t) values in the DSL sample reflect a moderate contribution

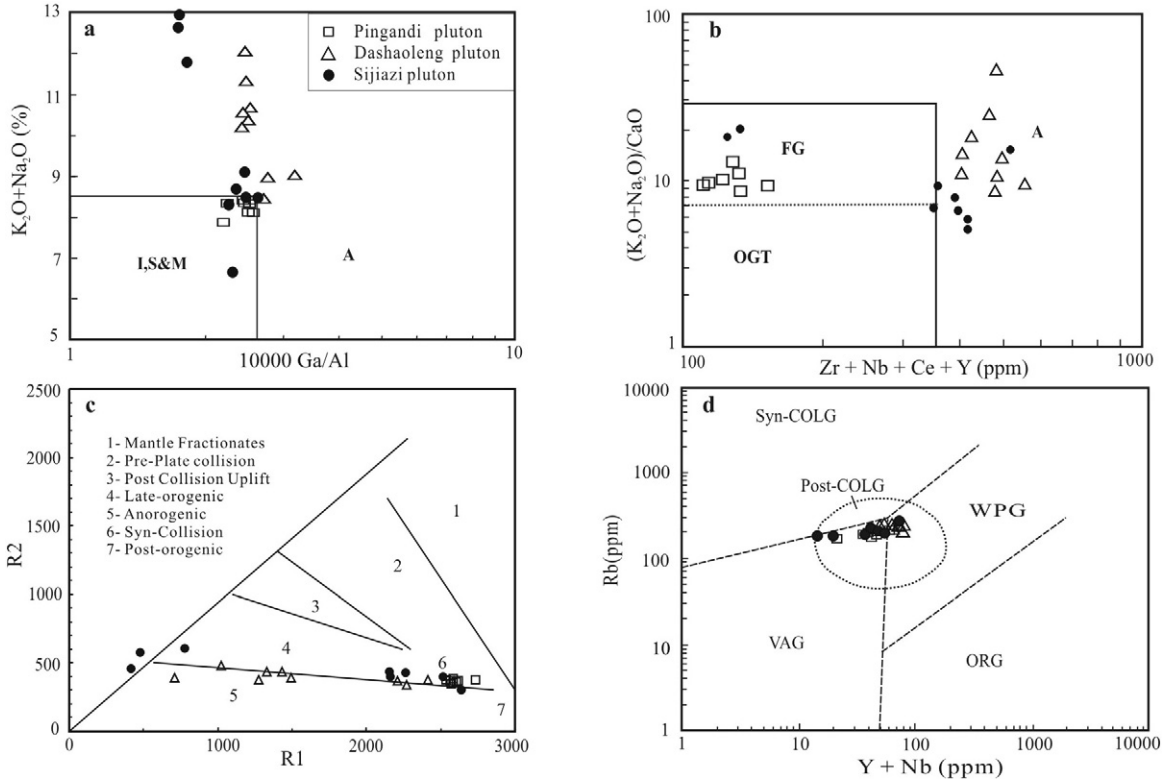

Fig. 7. (a) $K_2O + Na_2O$ vs. 10,000 Ga/Al discrimination diagram of Whalen et al. (1987), I, S & M = I-, S- and M-type granites. (b) $(K_2O + Na_2O)/CaO$ versus (Zr + Nb + Ce + Y) discrimination diagram of Whalen et al. (1987). FG = fractionated felsic granites, OGT = unfractionated I-, S- and M-type granites. (c) R2 (=6Ca + 2 Mg + Al) vs. R1 (=4Si − 11(Na + K) − 2(Fe + Ti)) diagram of Batchelor and Bowden (1985); (d) Rb vs. Y + Nb tectonic discrimination diagram of Pearce et al. (1984) and Pearce (1996). VAG = volcanic arc granites, WPG = within plate granites, COLG = collisional granites, ORG = oceanic ridge granites.

from juvenile mantle-derived source, while occasionally positive $\varepsilon_{Hf}(t)$ values in the SJZ samples diagnose a minor, much-diluted juvenile input. These magma archives for crustal growth of variable magnitude, plus the same period (260–220 Ma) of juvenile crustal record by the detrital zircons from the Xinglonggou Formation in western Liaoning (Meng et al., 2010), collectively witness a southwardly progressing crustal growth venue. This heralds a remarkable change in the crustal evolution of the northern NCC from reworking-dominated metacratonization during pre-latest Permian time (Zhang et al., 2011a, 2012a) to growth-oriented decratonization in latest Permian to Middle Triassic time.

The DSL and SJZ suites, plus a few recently-documented Triassic alkaline rocks (Yan et al., 2000; Ying et al., 2011), A-type granites (Han et al., 2004; Zhang et al., 2009a, 2012b) and shoshonitic dykes (Fu et al., 2012) from other areas, constitute an important alkaline magmatic belt along the northern NCC. This is distinct from predominant calc-alkaline magmatism during Carboniferous to early Late Permian time (Zhang et al., 2009a, 2011a, 2012a). Such an overall increase in granitoid alkalinity with time generally reflects the transition from post-collisional to within-plate settings (Bonin, 2004; Litvinovsky et al., 2011). This is consistent with current near-consensus that a post-orogenic extensional regime followed the final closure of Paleo-Asian Ocean and has prevailed in the northern NCC from latest Permian on (Fu et al., 2012; Meng et al., 2010; Xiao et al., 2003; Zhang et al., 2009a, 2010a, 2012b).

As in the case of the Iberian massif (Gutierrez-Alonso et al., 2011), the coupled change in magmatic and crustal evolutionary style during a time span of tens of millions years can be attributed to lithospheric dripping (Ducea, 2011), a small-scale variant of lithospheric delamination. Under such a scenario, asthenospheric upwelling and concomitant mafic magmatic underplating may have provided a heat supply and mantle-derived material at the crust–mantle boundary within the continental interior of the newly-amalgamated North China–Mongolian Plate. Continued mafic underplating could then lead to widespread crustal melting, resulting in the production of felsic magmas at different crustal levels. On one hand, those from the newly underplated protoliths experienced fractionation and ascended along pre-existing structures to the current level of emplacement to form ferroan granites with juvenile isotopic signatures and minimal crustal contamination, as represented by the PAD granites. On the other hand, mixing of depleted mantle-derived magma and their fractionated products, with old crustal-derived felsic melts would produce homogeneous hybrid magmas that moved into the middle crust and differentiated to form ferroan granites with mixed geochemical signatures, as represented by the DSL and SJZ suites.

These observations may offer fresh dimensions to hotly debated issue of the Mesozoic decratonization in the eastern NCC, which was initiated by comparative studies on the Ordovician kimberlite-borne and Tertiary basalt-borne mantle xenoliths leading to the proposition that 80–140 km of ancient, thick cratonic lithosphere was replaced by younger, thin and fertile lithospheric mantle (Griffin et al., 1998; Menzies et al., 1993; Yang et al., 2008b, 2010; Zheng et al., 2007). The documentation of juvenile magmatic input in the Middle to Late Triassic ferroan granitoids along the northern NCC indicates that such decratonization process may have progressed from the northern cratonic edge to the center since Late Permian on, much earlier than previously thought. This, coupled with similar patterns along the eastern edge outlined by Yang et al. (2008b, 2010), further suggests that diachronous decratonization pattern of the NCC may signify an episodic response of the craton to the evolving plate tectonic processes within two contrasting Phanerozoic orogenic systems (Collins et al., 2011). During most of the Paleozoic, the NCC is mainly involved in an asymmetrical internal orogenic system, which has the CAOB as one essential component and features predominantly N-directed subduction that led to fragmentation and collision of ancient continental fragments (Bahlburg, 2011; Collins et al., 2011). Superimposed on the long-term N-directed subduction scenario is transient, localized S-dipping subduction possibly triggered by intermittent slab flipping

during closure of backarc basins (Collins et al., 2011), as exemplified by a specific flipping case from north to south in the Solonker suture zone during Early Permian (Zhang et al., 2011b). It is this spike of S-dipping subduction that initiated the decratonization along the northern NCC. The lithospheric loss at the eastern edge was subsequently triggered by extension that followed collision between the Sino–Korean and Yangtze cratons (Yang et al., 2008b). Nevertheless, it is only when the NCC became a part of the external circum-Pacific orogenic system since the Jurassic that widespread destruction occurred in the eastern NCC (Zheng et al., 2007).

7. Conclusion

This study exemplifies a typical case of diverse ferroan granitoid magma genesis within a region of transitional tectonic affinity, with contrasting petrogenetic scenarios deciphered for each. The Middle Triassic PAD suite (c. 238 Ma) displays a dominant juvenile geochemical signature and argues for a partial melting scenario involving juvenile quartzofeldspathic crustal protoliths of CAOB affinity. By contrast, the Late Triassic (c. 220 Ma) DSL and SJZ suites show variably evolved geochemical signatures and are consistent with an origin by variable mixing between depleted mantle-derived mafic magma and old crustal-derived felsic magma, with a higher proportion of juvenile components manifest in the former. These contrasting ferroan granitoids constitute an essential part of the post-orogenic magmatic belt along the northern margin of the newly-amalgamated North China–Mongolian Plate. They not only serve as a spatial marker for monitoring the juxtaposition of the NCC and the CAOB along a lithospheric-scale boundary fault in the region, but also present a temporal snapshot for recording a southwardly-progressing crustal growth scenario possibly in response to lithospheric dripping within a post-orogenic extensional regime.

Supplementary materials related to this article can be found online at doi:10.1016/j.lithos.2012.03.022.

Acknowledgments

Our grateful acknowledgment goes to Qian Mao and Yuguang Ma for help with zircon CL imaging and mineral analysis; Yu Liu and Guoqiang Tang with SIMS analysis; He Li and Xindi Jin with major and trace element analysis; and Chaofeng Li with Sr–Nd isotope analysis. We are also grateful to Dr. G. Shellnutt, Prof. Nelson Eby and an anonymous reviewer for their constructive comments. This study was financially supported by the National Natural Science Foundation of China (Grant no. 90914008), the Major State Basic Research Program of the People's Republic of China (Grant no. 2012CB416603), the Knowledge Innovation Program of the Chinese Academy of Sciences (Grant no. KZCX2-YW-QN115) and the NNSFC Grant no. 40873026.

References

Bahlburg, H., 2011. Mantle-controlled mountains. Nature Geosciences 4, 280–282.
Batchelor, R.A., Bowden, P., 1985. Petrogenetic interpretation of granitoid rock series using multicationic parameters. Chemical Geology 48, 43–55.
Belousova, B.A., Griffin, W.L., O'Reilly, S.Y., 2006. Zircon crystal morphology, trace element signatures and Hf isotope composition as a tool for petrogenetic modelling: examples from Eastern Australian granitoids. Journal of Petrology 47, 329–353.
Bogaerts, M., Scaillet, B., Vander Auwera, J., 2006. Phase equilibria of the Lyngdal granodiorite (Norway): implications for the origin of metaluminous ferroan granitoids. Journal of Petrology 47, 2405–2431.
Bonin, B., 2004. Do coeval mafic and felsic magmas in post-collisional to within-plate regimes necessarily imply two contrasting, mantle and crustal, sources? A review. Lithos 78, 1–24.
Bonin, B., 2007. A-type granites and related rocks; evolution of a concept, problems and prospects. Lithos 97, 1–29.
Clemens, J.D., Darbyshire, D.P.F., Flinders, J., 2009. Sources of post-orogenic calc-alkaline magmas: the Arrochar and Garabal Hill-Glen Fyne complexes, Scotland. Lithos 112, 524–542.
Collins, W.J., Belousova, E.A., Kemp, A.I.S., Murphy, B., 2011. Two contrasting Phanerozoic orogenic systems revealed by hafnium isotope data. Nature Geosciences 4, 333–337.
Cope, T.D., Graham, S.A., 2007. Upper crustal response to Mesozoic tectonism in western Liaoning, North China, and implications for lithospheric delamination. In: Zhai, M.G., Windley, B.F., Kusky, T.M., Meng, Q.R. (Eds.), Mesozoic sub-continental lithospheric thinning under eastern Asia: Geological Society, London. Special Publication, vol. 280, pp. 201–222.
Davis, G.A., Zheng, Y., Wang, C., Darby, B.J., Zhang, C., Gehrels, G.E., 2001. Mesozoic tectonic evolution of the Yanshan fold and thrust belt, with emphasis on Hebei and Liaoning provinces, northern China. In: Hendrix, M.S., Davis, G.A. (Eds.), Paleozoic and Mesozoic tectonic evolution of central and eastern Asia: from continental assembly to intracontinental deformation: Geological Society of America Memoir, 194, pp. 171–197.
Ducea, M.N., 2011. Fingerprinting orogenic delamination. Geology 39, 191–192.
Frost, C.D., Frost, B.R., 1997. Reduced rapakivi-type granites: the tholeiite connection. Geology 25, 647–650.
Frost, C.D., Frost, B.R., 2011. On ferroan (A-type) granitoids: their compositional variability and modes of origin. Journal of Petrology 52, 39–53.
Frost, C.D., Bell, J.M., Frost, B.R., Chamberlain, K.R., 2001a. Crustal growth by magmatic underplating: isotopic evidence from the northern Sherman batholith. Geology 29, 515–518.
Frost, B.R., Barnes, C.G., Collins, W.J., Arculus, R.J., Ellis, D.J., Frost, C.D., 2001b. A geochemical classification for granitic rocks. Journal of Petrology 42, 2033–2048.
Fu, L., Wei, J., Kusky, T.M., Chen, H., Tan, J., Li, Y., Kong, L., Jiang, Y., 2012. Triassic shoshonitic dykes from the northern North China Craton: petrogenesis and geodynamic significance. Geological Magazine 149, 39–55.
Glazner, A.F., 2007. Thermal limitations on incorporation of wall rock into magma. Geology 35, 319–322.
Griffin, W.L., Zhang, A.D., O'Reilly, S.Y., Ryan, C.G., 1998. Phanerozoic evolution of the lithosphere beneath the Sino–Korean Craton. In: Flower, M.F.J., Chung, S.L., Lo, C.H., Lee, T.Y. (Eds.), Mantle dynamics and plate interactions in East Asia: American Geophysical Union, Geodynamics series, vol. 27, pp. 107–126.
Griffin, W.L., Wang, X., Jackson, S.E., Pearson, N.J., O'Reilly, S.Y., 2002. Zircon geochemistry and magma mixing, SE China: in-situ analysis of Hf isotopes, Tonglu and Pingtan igneous complexes. Lithos 61, 237–269.
Gutierrez-Alonso, G., Murphy, J.B., Fernández-Suárez, J., Weil, A.B., Franco, M.P., Gonzalo, J.P., 2011. Lithospheric delamination in the core of Pangea: Sm–Nd insights from the Iberian mantle. Geology 39, 155–158.
Han, B.F., Kagami, H., Li, H.M., 2004. Age and Nd–Sr isotopic geochemistry of the Guangtoushan alkaline granites, Hebei province, China: implications for early Mesozoic crust–mantle interaction in North China Block. Acta Petrologica Sinica 20, 1375–1388.
Jahn, B.M., 2004. The Central Asian Orogenic Belt and growth of the continental crust in the Phanerozoic. In: Malpas, J., Fletcher, C.J.N., Ali, J.R., Aitchison, J.C. (Eds.), Aspects of the tectonic evolution of China: Geological Society, London, Special Publications, 226, pp. 73–100.
Jian, P., Liu, D.Y., Kroner, A., Windley, B.F., Shi, Y.R., Zhang, W., Zhang, F.Q., Miao, L.C., Zhang, L., Tomurhuu, D., 2010. Evolution of a Permian intraoceanic arc–trench system in the Solonker suture zone, Central Asian Orogenic Belt, China and Mongolia. Lithos 118, 169–190.
Kemp, A.I.S., Hawkesworth, C.J., 2003. Granitic perspectives on the generation and secular evolution of the continental crust. In: Rudnick, R.L. (Ed.), Treatise on Geochemistry, The Crust 3. Elsevier Pergamon, Amsterdam, pp. 349–410.
Kemp, A.I.S., Wormald, R.J., Whitehouse, M.J., Price, R.C., 2005. Hf isotopes in zircon reveal contrasting sources and crystallization histories for alkaline to peralkaline granites of Temora, southeastern Australia. Geology 33, 797–800.
Kemp, A.I.S., Hawkesworth, C.J., Foster, G.L., Paterson, B.A., Woodhead, J.D., Hergt, J.M., Gray, C.M., Whitehouse, M.J., 2007. Magmatic and crustal differentiation history of granitic rocks from Hf–O isotopes in zircon. Science 315, 980–983.
Kusky, T.M., Windley, B.F., Zhai, M.G., 2007. Tectonic evolution of the North China Block: from orogen to craton to orogen. In: Zhai, M.G., Windley, B.F., Kusky, T.M., Meng, Q.R. (Eds.), Mesozoic sub-continental lithospheric thinning under eastern Asia: Geological Society, London. Special Publication, vol. 280, pp. 1–34.
Le Maitre, R.W., 2002. Igneous Rocks: A Classification and Glossary of Terms, 2nd edn. Cambridge University Press, Cambridge. 236 pp.
Li, X.H., Liu, Y., Li, Q.L., Guo, C.H., Chamberlain, K.R., 2009. Precise determination of Phanerozoic zircon Pb/Pb age by multi-collector SIMS without external standardization. Geochemistry Geophysical Geosystem 10, Q04010. doi:10.1029/2009GC00 2400.
Liaoning Bureau of Geology and Mineral Resources (LBGMR), 1971. 1:50000 scale geological map of Fuxin, Liaoning Province and the related notes. (in Chinese).
Liaoning Bureau of Geology and Mineral Resources (LBGMR), 1996. 1:50000 scale geological maps of the Jiumiao, Shabaotai and Haertao, Liaoning Province and the related notes. (in Chinese).
Litvinovsky, B.A., Tsygankov, A.A., Jahn, B.M., Katzir, Y., Be'eri-Shlevin, Y., 2011. Origin and evolution of overlapping calc-alkaline and alkaline magmas: the Late Palaeozoic post-collisional igneous province of Transbaikalia (Russia). Lithos 125, 845–874.
Liu, S.W., Santosh, M., Wang, W., Bai, X., Yang, P.T., 2011. Zircon U–Pb chronology of the Jianping Complex: implications for the Precambrian crustal evolution history of the northern margin of North China Craton. Gondwana Research 20, 48–63.
Lugmair, G.W., Marti, K., 1978. Lunar initial 143Nd/144Nd: differential evolution of the lunar crust and mantle. Earth and Planetary Science Letters 39, 349–357.
Meng, F.X., Gao, S., Yuan, H.L., Gong, H., 2010. Permian–Triassic (260–220 Ma) crustal growth of eastern central Asian orogenic belt as revealed by detrital zircon studies. American Journal of Science 310, 364–404.
Menzies, A., Fan, W.M., Zhang, M., 1993. Paleozoic and Cenozoic lithoprobes and the loss of >120 km of Archean lithosphere, Sino–Korean Craton, China. In: Prichard, H.M. (Ed.), Magmatic processes and plate tectonics: Geological Society [London] Special Publications, vol. 76, pp. 71–81.

Mushkin, A., Navon, O., Halicz, L., Hartmann, G., Stein, M., 2003. The petrogenesis of A-type magmas from the Amram Massif, southern Israel. Journal of Petrology 44, 815–832.
Patiño Douce, A.E., 1997. Generation of metaluminous A-type granites by low-pressure melting of calc-alkaline granitoids. Geology 25, 743–746.
Pearce, J.A., 1996. Sources and settings of granitic rocks. Episodes 19, 120–125.
Pearce, R.R., Harris, N.B.W., Tindle, A.G., 1984. Trace element discrimination diagrams for the tectonic interpretation of granitic rocks. Journal of Petrology 25, 956–983.
Pitcher, W.S., 1993. The Nature and Origin of Granite. Blackie Academic and Professional, London. 321 pp.
Shaw, S.E., Flood, R.H., 2009. Zircon Hf isotopic evidence for mixing of crustal and silicic mantle-derived magmas in a zoned granite pluton, Eastern Australia. Journal of Petrology 50, 147–168.
Sisson, T.W., Ratajesti, K., Hankins, W.B., Glazner, A.F., 2005. Voluminous granitic magmas from common basaltic sources. Contributions to Mineralogy and Petrology 148, 635–661.
Skjerlie, K.P., Johnston, A.D., 1993. Fluid-absent melting behavior of an F-rich tonalitic gneiss at mid-crustal pressures: implications for the generation of anorogenic granites. Journal of Petrology 34, 785–815.
Steiger, R.H., Jäger, E., 1977. Subcommission on geochronology; convention on the use of decay constants in geochronology and cosmochronology. Earth and Planetary Science Letters 36, 359–362.
Sun, S.S., McDonough, W.F., 1989. Chemical and isotopic systematics of oceanic basalts: implications for mantle composition and processes. In: Saunders, A.D., Norry, M.J. (Eds.), Magmatism in the Ocean Basins: Geological Society, London, Special Publications, 42, pp. 528–548.
Wang, W., Liu, S.W., Bai, X., Yang, P., Li, Q., Zhang, L., 2011. Geochemistry and zircon U–Pb–Hf isotopic systematics of the Neoarchean Yixian–Fuxin greenstone belt, northern margin of the North China Craton: implications for petrogenesis and tectonic setting. Gondwana Research 20, 64–81.
Whalen, J.B., Currie, K.L., Chappell, B.W., 1987. A-type granites: geochemical characteristics, discrimination and petrogenesis. Contributions to Mineralogy and Petrology 95, 407–419.
Whitaker, M.L., Nekvasil, H., Lindsley, D.H., McCurry, M., 2008. Can crystallization of olivine tholeiite give rise to potassic rhyolites — an experimental investigation. Bulletin of Volcanology 70, 417–434.
Windley, B.F., Alexeiev, D., Xiao, W.J., Kroner, A., Badarch, G., 2007. Tectonic models for accretion of the Central Asian Orogenic Belt. Journal of the Geological Society of London 164, 31–47.
Woodhead, J.D., Hergt, J., Shelley, M., Eggins, S., Kemp, R., 2004. Zircon Hf-isotope analysis with an excimer laser, depth profiling, ablation of complex geometries, and concomitant age estimation. Chemical Geology 209, 121–135.
Wu, F.Y., Yang, Y.H., Xie, L.W., Yang, J.H., Xu, P., 2006. Hf isotopic compositions of the standard zircons and baddeleyites used in U–Pb geochronology. Chemical Geology 234, 105–126.
Xiao, W., Windley, B.F., Hao, J., Zhai, M., 2003. Accretion leading to collision and the Permian Solonker suture, Inner Mongolia, China: termination of the Central Asian Orogenic Belt. Tectonics 22, 1484–1505.
Yan, G., Mu, B., Xu, B., He, G., Tan, L., Zhao, H., He, Z., 2000. Geochronology and isotopic features of Sr, Nd, and Pb of the Triassic alkali intrusions in the Yanshan–Yinshan regions. Science in China, Series D: Earth Sciences 30, 384–387.
Yang, J.H., Wu, F.Y., Shao, J.A., Wilde, S.A., Xie, L.W., Liu, X.M., 2006. Constraints on the timing of uplift of the Yanshan fold and thrust belt, North China Craton. Earth and Planetary Science Letters 246, 336–352.
Yang, J.H., Wu, F.Y., Wilde, S.A., Chen, F.K., Liu, X.M., Xie, L.W., 2008a. Petrogenesis of an alkali syenites–granite–rhyolite suite in the Yanshan fold and thrust belt, eastern North China Craton: geochronological, geochemical and Nd–Sr–Hf isotopic evidence for lithospheric thinning. Journal of Petrology 49, 315–351.
Yang, J.H., Wu, F.Y., Wilde, S.A., Belousova, E., Griffin, W.L., 2008b. Mesozoic decratonization of the North China Block. Geology 36, 467–470.
Yang, Y.H., Wu, F.Y., Wilde, S.A., Liu, X.M., Zhang, Y.B., Xie, L.W., Yang, J.H., 2009. In situ perovskite Sr–Nd isotopic constraints on the petrogenesis of the Ordovician Mengyin kimberlites in the North China Craton. Chemical Geology 264, 24–42.
Yang, J.H., O'Reilly, S., Walker, R.J., Griffin, W., Wu, F.Y., Zhang, M., Pearson, N., 2010. Diachronous decratonization of the Sino–Korean Craton: geochemistry of mantle xenoliths from North Korea. Geology 38, 799–802.
Ying, J.F., Zhang, H.F., Tang, Y.J., 2011. Crust–mantle interaction in the central North China Craton during the Mesozoic: evidence from zircon U–Pb chronology, Hf isotope and geochemistry of syenitic–monzonitic intrusions from Shanxi province. Lithos 125, 449–462.
Zhang, X.H., Zhai, M.G., 2010. Magmatism and its metallogenetic effects during the Paleozoic continental crustal construction in northern North China: an overview. Acta Petrologica Sinica 26, 1329–1341.
Zhang, X.H., Zhang, H.F., Tang, Y.J., Wilde, S.A., Hu, Z.C., 2008a. Geochemistry of Permian bimodal volcanic rocks from Central Inner Mongolia, North China: implication for tectonic setting and Phanerozoic continental growth in Central Asian Orogenic Belt. Chemical Geology 249, 261–281.
Zhang, X.H., Mao, Q., Zhang, H.F., Wilde, S.A., 2008b. A Jurassic peraluminous leucogranite from Yiwulüshan, western Liaoning, North China Craton: age, origin and tectonic significance. Geological Magazine 145, 305–320.
Zhang, S.H., Zhao, Y., Song, B., Hu, J.M., Liu, S.W., Yang, Y.H., Chen, F.K., Liu, X.M., Liu, J., 2009a. Contrasting Late Carboniferous and Late Permian–Middle Triassic intrusive suites from the northern margin of the North China Craton: geochronology, petrogenesis and tectonic implications. Geological Society of America Bulletin 121, 181–200.
Zhang, S.H., Zhao, Y., Liu, X.C., Liu, D.Y., Chen, F.K., Xie, L.W., Chen, H.H., 2009b. Late Paleozoic to Early Mesozoic mafic–ultramafic complexes from the northern North China Block: constraints on the composition and evolution of the lithospheric mantle. Lithos 110, 229–246.
Zhang, X.H., Zhang, H.F., Zhai, M.G., Wilde, S.A., Xie, L.W., 2009c. Geochemistry of middle Triassic gabbros from northern Liaoning, North China: origin and tectonic implications. Geological Magazine 146, 540–551.
Zhang, X.H., Zhang, H.F., Wilde, S.A., Yang, Y.H., Chen, H.H., 2010a. Late Permian to early Triassic mafic to felsic intrusive rocks from North Liaoning, North China: petrogenesis and implication for Phanerozoic continental growth. Lithos 117, 283–306.
Zhang, X.H., Zhang, H.F., Jiang, N., Zhai, M.G., Zhang, Y.B., 2010b. Early Devonian alkaline intrusive complex from the northern North China Craton: a petrologic monitor of post-collisional tectonics. Journal of the Geological Society of London 167, 717–730.
Zhang, X.H., Wilde, S.A., Zhang, H.F., Zhai, M.G., 2011a. Early Permian high-K calc-alkaline volcanic rocks from northwest Inner Mongolia, North China: geochemistry, origin and tectonic implications. Journal of the Geological Society of London 168, 525–543.
Zhang, X.H., Mao, Q., Zhang, H.F., Zhai, M.G., Yang, Y., Hu, Z., 2011b. Mafic and felsic magma interaction during the construction of high-K calc-alkaline plutons within a metacratonic passive margin: the early Permian Guyang batholith from the northern North China Craton. Lithos 125, 569–591.
Zhang, X.H., Gao, Y.L., Wang, Z.J., Liu, H., Ma, Y.G., 2012a. Carboniferous appinitic intrusions from the northern North China Craton: geochemistry, petrogenesis and tectonic implications. Journal of the Geological Society of London 169. doi:10.1144/0016-76492011-062.
Zhang, Z., Zhang, H.F., Shao, J., Ying, J.F., Yang, Y.H., Santosh, M., 2012b. Guangtoushan granites and their enclaves: implications for Triassic mantle upwelling in the northern margin of the North China Craton. Lithos. doi:10.1016/j.lithos.2011.11.018.
Zhao, G.C., Wilde, S.A., Cawood, P.A., Sun, M., 2001. Archean blocks and their boundaries in the North China Craton: lithological, geochemical, structural and P–T path constraints and tectonic evolution. Precambrian Research 107, 45–73.
Zheng, J.P., Griffin, W.L., O'Reilly, S.Y., Yu, C.M., Zhang, H.F., Pearson, N., Zhang, M., 2007. Mechanism and timing of lithospheric modification and replacement beneath the eastern North China Craton: peridotitic xenoliths from the 100 Ma Fuxin basalts and a regional synthesis. Geochimica et Cosmochimica Acta 71, 5203–5225.